Experimental and Theoretical Study of the Atmospheric Chemistry and Global Warming Potential of SO_2F_2

Vassileios C. Papadimitriou,[†,‡] **R. W. Portmann,**[†] **David W. Fahey,**[†] **Jens Mühle,**[§] **Ray F. Weiss,**[§] **and James B. Burkholder***[,†]

Chemical Sciences Division, Earth System Research Laboratory, National Oceanic and Atmospheric Administration, 325 Broadway, Boulder Colorado, 80305-3328, Cooperative Institute for Research in Environmental Sciences, University of Colorado, Boulder, Colorado, 80309, and Scripps Institution of Oceanography, University of California, San Diego, La Jolla, California 92093-0244

In this work, potential atmospheric loss processes for SO_2F_2, a commercially used biocide (fumigant), have been studied and its global warming potential calculated. Rate coefficients for the gas-phase reactions OH + $SO_2F_2 \rightarrow$ products, k_1, and Cl + $SO_2F_2 \rightarrow$ products, k_4, were determined using a relative rate technique to be $k_1 < 1 \times 10^{-16}$ cm³ molecule⁻¹ s⁻¹ at 296 and 333 K and k_4(296 K) $< 5 \times 10^{-17}$ cm³ molecule⁻¹ s⁻¹. UV absorption cross sections of SO_2F_2 were measured at 184.9, 193, and 213.9 nm, and its photolysis quantum yield at 193 nm was determined to be <0.02. The atmospheric lifetime of SO_2F_2 with respect to loss by OH, Cl, and O(^{1}D) reaction and UV photodissociation is estimated to be >300, >10 000, 700, and >4700 years, respectively. The stratospheric lifetime of SO_2F_2 is calculated using a two-dimensional model to be 630 years. The global warming potential (GWP) for SO_2F_2 was calculated to be 4780 for the 100 year time horizon using infrared absorption cross sections measured in this work and a SO_2F_2 globally averaged atmospheric lifetime of 36 years, which is determined primarily by ocean uptake, reported by Mühle et al. (Mühle, J.; Huang, J.; Weiss, R. F.; Prinn, R. G.; Miller, B. R.; Salameh, P. K.; Harth, C. M.; Fraser, P. J.; Porter, L. W.; Greally, B. R.; O'Doherty, S.; Simonds, P. G. *J. Geophys. Res.*, submitted for publication, 2008). Reaction channels and the possible formation of stable adducts in reactions 1 and 4 were evaluated using ab initio, CCSD(T), and density functional theory, B3P86, quantum mechanical electronic structure calculations. The most likely reaction product channels were found to be highly endothermic, consistent with the upper limits of the rate coefficients measured in this work.

Introduction

Sulfuryl fluoride, SO_2F_2, is a high-vapor-pressure biocide that is primarily used as a commercial fumigant (wood preservative and insecticide). SO_2F_2 is currently being used as an alternative to methyl bromide, CH_3Br, whose use was regulated under the Montreal protocol (1986) due to its contribution to stratospheric ozone loss. Although SO_2F_2 has been commercially available since the 1960s, its atmospheric abundance and rate of increase have only recently been quantified as part of the Advanced Global Atmospheric Gases Experiment (AGAGE) global measurement program.[1] SO_2F_2 has a negligible ozone depletion potential but is a greenhouse gas and has the potential to be a radiative forcing agent. An evaluation of the potential impact of SO_2F_2 on climate requires a thorough understanding of its atmospheric loss processes and lifetime, which were not well-characterized before this study.[2,3]

Typical loss processes for atmospheric trace gases normally include gas-phase reaction with species such as O(^{1}D), Cl, OH, O_3, or NO_3, UV−vis photolysis, wet or dry deposition, or heterogeneous processes. Sulfuryl fluoride is expected to have low atmospheric gas-phase reactivity due to its chemical stability, i.e., large S=O and S−F bond strengths. In a recent study, rate coefficients, k, for the SO_2F_2 gas-phase reactions

$$OH + SO_2F_2 \rightarrow products \quad (1)$$

and

$$O_3 + SO_2F_2 \rightarrow products \quad (2)$$

were reported to be k_1(294 K) $< 1 \times 10^{-15}$ cm³ molecule⁻¹ s⁻¹ and k_2(294 K) $< 1 \times 10^{-23}$ cm³ molecule⁻¹ s⁻¹.[4] The reported upper limit for the O_3 rate coefficient establishes that this reaction represents a negligible atmospheric loss process for SO_2F_2. The upper limit for k_1, however, corresponds to an atmospheric lifetime for reaction with OH, τ_{OH}, of ~30 years, and hence, reaction 1 could be a significant atmospheric loss process for SO_2F_2. A more accurate determination of k_1 is needed to better define τ_{OH}.

SO_2F_2 is volatile and has low solubility in aqueous solutions with pH < 7[2] and, therefore, does not partition efficiently into atmospheric aerosol. SO_2F_2 does, however, react in alkaline solutions via

$$SO_2F_2 + OH^- \rightarrow HOSO_2F + F^- \quad (3)$$

that makes atmospheric loss by ocean uptake a potentially important process. Mühle et al.[1] reported the SO_2F_2 lifetime with respect to ocean uptake to be 40 (±13) years. Atmospheric loss of SO_2F_2 via UV photolysis[5] and reaction with O(^{1}D)[4] are only expected to be significant in the stratosphere, thus leading to relatively long lifetimes as a result of the slow turnover of the atmosphere through the stratosphere.

---

* Corresponding author. E-mail: James.B.Burkholder@noaa.gov.
† National Oceanic and Atmospheric Administration.
‡ CIRES, University of Colorado.
§ Scripps Institution of Oceanography.

Here, we report laboratory measurements of the rate coefficients for the gas-phase reaction of OH, k_1, and Cl atoms, k_4, with SO_2F_2:

$$Cl + SO_2F_2 \rightarrow products \qquad (4)$$

We also have studied the UV photolysis SO_2F_2 by measuring its absorption cross section at 184.9, 193, and 214 nm and its photolysis quantum yield at 193 nm. An evaluation of the SO_2F_2 atmospheric loss processes and associated lifetimes are presented as well as the global warming potential (GWP) of SO_2F_2 that was determined using SO_2F_2 infrared absorption spectra measured in this work. In addition, the heats of reaction, $\Delta_r H$, for possible product channels in reactions 1 and 4 have been evaluated using quantum chemical calculations. Geometries and frequencies were calculated at the MP2/6-31++G(d′,p′) level of theory, whereas absolute electronic energies were determined using density functional theory (DFT), B3P86 and B3PW91, and ab initio methods, CCSD(T).

Experimental Details

The experimental work presented here consisted of several independent studies that include (1) SO_2F_2 UV and infrared absorption cross sections in the gas phase, (2) rate coefficient measurements, using a relative rate technique, for the reaction of OH and Cl atoms with SO_2F_2, and (3) measurements of the SO_2F_2 photolysis quantum yield at 193 nm. Details of the experimental apparatus and methods used for these measurements are described separately in the following sections.

Absorption Cross Section Measurements. Gas-phase UV absorption cross sections for SO_2F_2 were measured at 184.9, 193, and 213.9 nm and infrared spectra were measured between 500 and 4000 cm^{-1}. Absorption cross sections were determined using absolute pressure measurements of either pure SO_2F_2 or manometrically prepared mixtures of SO_2F_2 in He. Absorption was measured for a range of SO_2F_2 concentrations, and cross sections were determined using Beer–Lambert's law

$$A = -\ln\left(\frac{I(\lambda)}{I_0(\lambda)}\right) = \sigma_\lambda L[SO_2F_2] \qquad (5)$$

where A is the measured absorbance (integrated infrared absorbance), $I(\lambda)$ and $I_0(\lambda)$ are the measured light intensity at wavelength λ with and without SO_2F_2 in the absorption cell, σ is the SO_2F_2 absorption cross section (integrated band strength, S), L the optical path length, and $[SO_2F_2]$ the SO_2F_2 concentration. Infrared absorption spectra were recorded at resolutions of 0.125, 0.25, 0.5, and 1.0 cm^{-1} using a Fourier transform spectrometer. The UV absorption cross sections were measured using Hg (184.9 nm) and Zn (213.9 nm) atomic resonance lamps and a low-energy pulsed ArF excimer laser (193 nm).

The 184.9 nm SO_2F_2 absorption cross section was measured using a 50 cm long absorption cell, a Hg Pen-Ray lamp light source, and a solar blind phototube detector. Eight different SO_2F_2 concentrations in the range of $0.37-2.52 \times 10^{17}$ molecule cm^{-3} were used in the cross section determination. The SO_2F_2 absorption cross section at 193 nm was measured using a low-energy pulsed ArF excimer laser (~ 0.1 mJ cm^{-2} pulse^{-1}) light source whose intensity was measured with a calibrated power meter at the exit of a 100 cm long absorption cell. The SO_2F_2 concentration was varied over the range of $0.06-1.15 \times 10^{18}$ molecule cm^{-3} in the 193 nm cross section determination. The SO_2F_2 absorption cross section at 213.9 nm (Zn lamp) was measured using a 130 cm long absorption cell and a phototube detector with a 214 nm narrow band-pass filter. Fourteen SO_2F_2 concentrations in the range of $0.78-9.8 \times 10^{18}$ molecule cm^{-3}

were used. For the 193 and 213.9 nm cross section determinations, pure SO_2F_2 samples were used and its concentration was determined from absolute pressure measurements using calibrated pressure meters.

Infrared absorption cross sections were determined using a 15 cm long absorption cell and SO_2F_2 concentrations in the range of $0.91-7.48 \times 10^{15}$ molecule cm^{-3}. The SO_2F_2 infrared absorption spectrum was found to be independent of bath gas pressure over the pressure range of $25-205$ Torr (He).

Quantum Yield Measurements. The SO_2F_2 photolysis quantum yield was measured using methods similar to those used in a previous study of acetone quantum yields in this laboratory.[6] The photolysis quantum yield of SO_2F_2 was measured by exposing a SO_2F_2 sample, in either a He or N_2 bath gas, to the output of a 193 nm (ArF excimer) pulsed laser. The loss of SO_2F_2 in the sample was measured using infrared absorption. The fraction of SO_2F_2 lost per photolysis laser pulse was small, $\sim 2 \times 10^{-7}$; therefore, the sample was exposed to multiple laser pulses prior to measuring the loss of SO_2F_2.

Quantum yields were measured using the following procedure. First, the photolysis and infrared absorption cells were filled with a SO_2F_2/bath gas mixture and the SO_2F_2 concentration was measured by infrared absorption. The sample in the photolysis cell was exposed to a measured number of pulses from the photolysis laser while the sample was being circulated between the photolysis and absorption cells using a 20 L min^{-1} Teflon-coated pump. The SO_2F_2 concentration was then measured, and the sample photolysis was repeated. The photolysis procedure was repeated at least five times for each sample. Photolysis cells with path lengths of 100 cm and internal diameters of 1.5 and 5 cm were used during the course of the experiments (the measured SO_2F_2 photolysis quantum yield was independent of the surface-to-volume ratio). The laser beam passed along the length of the photolysis cell but did not fill the cross sectional area (volume) of the cell. The photolysis laser fluence was measured with a power meter at the exit of the photolysis cell.

The concentration of SO_2F_2 remaining after "n" laser pulses is given by

$$[SO_2F_2]_n = [SO_2F_2]_0[1 - \sigma_{193nm}^{SO_2F_2}\Phi F]^n \qquad (6)$$

where $[SO_2F_2]_0$ is the initial SO_2F_2 concentration, $\sigma_{193nm}^{SO_2F_2}$ is the absorption cross section of SO_2F_2 at 193 nm, Φ is the photolysis quantum yield of SO_2F_2, and F is the photolysis laser fluence. A linear least-squares analysis of $\ln([SO_2F_2]_n/[SO_2F_2]_0)$ versus n

$$\ln\left(\frac{[SO_2F_2]_n}{[SO_2F_2]_0}\right) = -n\ln(1 - \sigma_{193nm}^{SO_2F_2}\Phi F) \qquad (7)$$

yields $\ln(1 - \sigma_{193nm}^{SO_2F_2}\Phi F)$, and Φ was calculated using the SO_2F_2 absorption cross section at 193 nm and the calibrated laser fluence.

The photolysis laser fluence was calibrated using N_2O as a reference photolyte

$$N_2O + h\nu \rightarrow O(^1D) + N_2 \qquad (8)$$
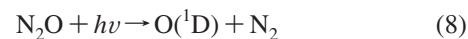
where the N_2O quantum yield at 193 nm is unity.[7] N_2O photolysis measurements were performed using a N_2 bath gas (600 Torr) such that $O(^1D)$ produced in reaction 8 was rapidly quenched to its ground state:

$$O(^1D) + N_2 \rightarrow O(^3P) + N_2 \qquad (9)$$
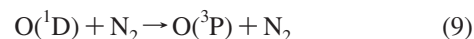
The calibration experiments used the same methods as the SO_2F_2 photolysis measurements, and the change in the N_2O concentration was measured using infrared absorption.

Atmospheric Chemistry and GWP of SO$_2$F$_2$

J. Phys. Chem. A, Vol. xxx, No. xx, XXXX **C**

SO$_2$F$_2$ quantum yields were measured in He and N$_2$ bath gases at pressures between 60 and 620 Torr. The photolysis laser fluence was varied over the range of 2−10 mJ cm^{-2} pulse^{-1}. The initial SO$_2$F$_2$ and N$_2$O concentrations were varied between 2 and 8 × 10^{15} molecule cm^{-3} and 1 and 2 × 10^{16} molecule cm^{-3}, respectively. The photolysis laser was operated at 20 Hz, and all measurements were performed at 296 K.

Rate Coefficient Measurements. Rate coefficients for the gas-phase reactions of SO$_2$F$_2$ with OH and Cl were measured using a relative rate method. The loss of SO$_2$F$_2$ and a reference compound, for which the rate coefficient is known, were measured using infrared absorption. Provided that SO$_2$F$_2$ and the reference compound are lost solely due to OH or Cl atom reaction the rate coefficients are related by

$$\ln\left(\frac{[SO_2F_2]_0}{[SO_2F_2]_t}\right) = \frac{k_i}{k_{Ref}}\ln\left(\frac{[Ref]_0}{[Ref]_t}\right) \tag{10}$$

where [SO$_2$F$_2$]$_0$ and [Ref]$_0$ are the initial concentrations of SO$_2$F$_2$ and the reference compound and [SO$_2$F$_2$]$_t$ and [Ref]$_t$ are the concentrations at time t.

OH radicals were produced by the 248 nm pulsed laser photolysis (KrF excimer, 10−20 Hz) of ozone

$$O_3 + h\nu \rightarrow O(^1D) + O_2(^1\Delta) \tag{11a}$$

$$\rightarrow O(^3P) + O_2(^3\Sigma) \tag{11b}$$
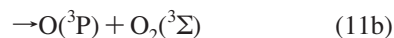
in the presence of a large excess of H$_2$O (∼19 Torr) in a He bath gas. The yield of the electronically excited oxygen atoms, O(^{1}D), in reaction 11 is 0.9.[7] OH radicals are produced in the reaction

$$O(^1D) + H_2O \rightarrow 2OH \tag{12}$$

where k_{12}(298 K) = 2.0 × 10^{-10} cm^3 molecule^{-1} s^{-1}.[7] Rate coefficient measurements were measured using the experimental setup described in the photolysis quantum yield experiments (using the larger volume cell, gas residence time ≈6 s) with the loss of the sample and reference compounds measured via infrared absorption. The temperature of the reactor was maintained by circulating fluid from a temperature-regulated reservoir through the reactors jacket. The temperature of the gas at the entrance and exit of the reactor was measured to be within 1 °C of that of the circulating fluid. The infrared cell and gas circulation manifold were at room temperature.

We have used CHF$_3$ as the reference compound

$$OH + CHF_3 \rightarrow products \tag{13}$$
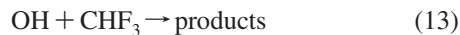
in studying reaction 1 where $k_{13}(T)$ = 6.3 × 10^{-13} exp(−2300/T) cm^3 molecule^{-1} s^{-1}; k_{13}(298 K) = 2.8 × 10^{-16} cm^3 molecule^{-1} s^{-1}.[7] Rate coefficients were measured by first adding SO$_2$F$_2$, CHF$_3$, H$_2$O, and He bath gas to the reactor. The contents were thoroughly mixed, and the SO$_2$F$_2$ and CHF$_3$ concentrations were measured by infrared absorption. The total pressure of the initial gas mixture in the reactor was ∼100 Torr. During the course of the rate coefficient measurements, the initial concentrations of SO$_2$F$_2$, CHF$_3$, and H$_2$O were varied over the ranges of 2−8 × 10^{15}, 2.8−6.5 × 10^{15}, and 3−6 × 10^{17} molecule cm^{-3}, respectively. Following the complete mixing of the sample, ozone was slowly added to the reaction mixture while the UV photolysis laser was passing through the reactor.

The ozone concentration in the reactor was kept low in order to minimize the loss of OH radicals produced in reaction 12 by reaction with ozone

$$OH + O_3 \rightarrow HO_2 + O_2 \tag{14}$$
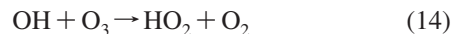
where $k_{14}(T)$ = 1.7 × 10^{-12} exp(−940/T) cm^3 molecule^{-1} s^{-1} and k_{14}(298 K) = 7.3 × 10^{-14} cm^3 molecule^{-1} s^{-1}.[7] The steady-state concentration of ozone in the reactor was <5 × 10^{12} molecule cm^{-3} in all experiments. It should be noted that the loss of OH via reaction 14 does not influence our relative rate measurement provided that the extent of reactions 1 and 13 are sufficient to yield measurable changes in the concentrations of the reference and sample compounds.

An additional consideration in our OH relative rate measurement is the possible loss of the reference and/or sample compounds by reaction with O(^{1}D)

$$O(^1D) + SO_2F_2 \rightarrow products \tag{15a}$$

$$\rightarrow O(^3P) + SO_2F_2 \tag{15b}$$

$$O(^1D) + CHF_3 \rightarrow products \tag{16a}$$

$$\rightarrow O(^3P) + CHF_3 \tag{16b}$$

where k_{15}(298 K) = 1.3 × 10^{-10} cm^3 molecule^{-1} s^{-1}, k_{15b}(298 K) = 5.8 × 10^{-11} cm^3 molecule^{-1} s^{-1} [4], k_{16}(298 K) = 9.1 × 10^{-12} cm^3 molecule^{-1} s^{-1}, and the branching ratio favors collisional quenching, k_{16b}/k_{16} > 0.75.[7] The collisional quenching of O(^{1}D) by the reactants, reactions 15b and 16b, will not influence the relative rate measurement because the reactants are not lost by this process. However, O(^{1}D) reactive loss, reactions 15a and 16a, will influence the relative rate measurement. The use of high H$_2$O and the lowest possible reactant concentrations minimizes the extent to which reactions 15 and 16 occur. The H$_2$O pressure was varied during the course of our experiments between 5 and 20 Torr. The limitations on our k_1 rate coefficient determination imposed by the O(^{1}D) reaction is discussed in the Results and Discussion section.

CH$_2$FCF$_3$ (HFC-134a) was used as a reference in our Cl atom relative rate measurements

$$Cl + CH_2FCF_3 \rightarrow products \tag{17}$$

where k_{17}(298 K) = 1.5 × 10^{-15} cm^3 molecule^{-1} s^{-1} with an estimated uncertainty of 10%.[7] Cl atoms were generated by the 351 nm (XeF excimer laser) pulsed laser photolysis of Cl$_2$:

$$Cl_2 + h\nu \rightarrow 2Cl \tag{18}$$

Rate coefficients were measured using nearly the same methodology as in the OH experiments. Cl$_2$ (0.2−2 × 10^{17} molecule cm^{-3}) was added to the initial reaction mixture and the pressure of the reactor was 630 Torr with N$_2$ as the bath gas. The initial concentrations of the reference compound and SO$_2$F$_2$ were ∼4.5 × 10^{16} molecule cm^{-3}. In several measurements, 20 Torr of O$_2$ was added to the gas mixture.

Materials. The SO$_2$F$_2$ gas sample (99.8% purity) used in this study was stored in a vacuum-sealed stainless steel container. The SO$_2$F$_2$ sample was degassed using several freeze− pump−thaw cycles prior to use. Either pure SO$_2$F$_2$ or dilute mixtures of SO$_2$F$_2$ in He (0.11 and 1.3%), prepared manometrically in a 12 L Pyrex bulb, were used during the course of this study. The SO$_2$F$_2$ abundance in the prepared mixtures was measured using infrared absorption and was stable for at least 2 months. Ozone was produced by flowing O$_2$ through a commercial ozonizer and collected on silica gel in a trap at 195 K. Ozone was introduced into the reaction cell by passing a small flow of He through the trap before entering the reactor. He (UHP, 99.999%), O$_2$(UHP, 99.99%), Syn. Air (80% N$_2$/ 20% O$_2$), and Cl$_2$, a mixture containing 0.2% Cl$_2$ in He, were

TABLE 1: UV Absorption Cross Sections for SO_2F_2 at 296 K Measured in This Work

wavelength (nm)	cross section $(10^{-22} cm^2 molecule^{-1})^a$
184.9	71.7 ± 1.2
193	40 ± 4.4
213.9	2.08 ± 0.04

^{a} The uncertainties are 2σ (95% confidence level) and were obtained from the precision and the estimated absolute uncertainty in the absorption measurement.
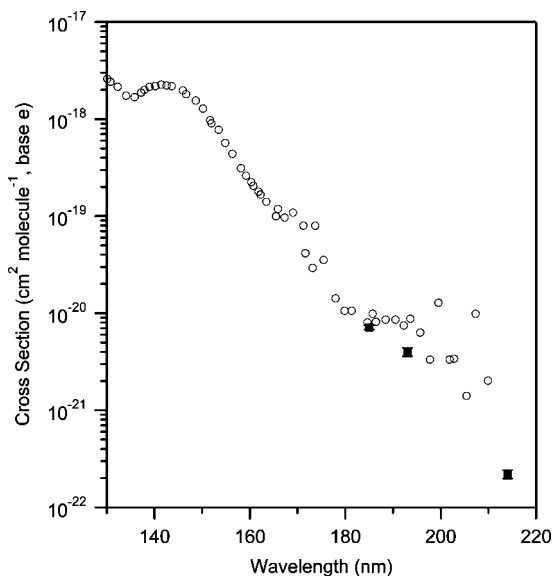

Figure 1. UV absorption cross sections of SO_2F_2 measured at 184.9, 193, and 213.9 nm in this work (●). The error bars are the 2σ values of the precision of the measurements. The UV absorption spectrum reported in Pradayrol et al. (ref 5) (○) is included for comparison.

used as supplied. Distilled H_2O was degassed, stored in a Pyrex vacuum reservoir, and introduced directly into the reactor from the headspace of the reservoir. CH_2FCF_3 (99.995%), CHF_2CF_3 (>99.99%), and CHF_3 (>99.9%) were used as reference compounds in the OH and Cl rate coefficient determinations. Pressure was measured using 10 and 1000 Torr capacitance manometers.

Results and Discussion

UV Absorption Spectrum. Gas-phase UV absorption cross sections for SO_2F_2 measured at 184.9, 193, and 213.9 nm are listed in Table 1. Over this wavelength range, the SO_2F_2 absorption cross sections are relatively small and decrease with increasing wavelength. A comparison of our results with the SO_2F_2 UV absorption spectrum reported by Pradayrol et al.[5] (the only other UV cross section data currently available in the literature) over the wavelength range of 130−210 nm is given in Figure 1. Note, we have extracted the Pradayrol et al. absorption cross section data from Figure 5 in their paper which may have introduced some small error in the values we report from their study. Our absorption cross section measured at 184.9 nm, $(7.17 \pm 0.12) \times 10^{-21} cm^2 molecule^{-1}$, is in good agreement with the value from the Pradayrol et al.,[5] ∼$8 \times 10^{-21} cm^2 molecule^{-1}$, study. Our absorption cross sections at 193 and 213.9 nm, $(4.08 \pm 0.44) \times 10^{-21}$ and $(2.08 \pm 0.04) \times 10^{-22} cm^2 molecule^{-1}$, respectively, are lower than given in Pradayrol et al. The quoted uncertainties in our absorption cross sections are at the 2σ level and include estimated systematic errors. Our
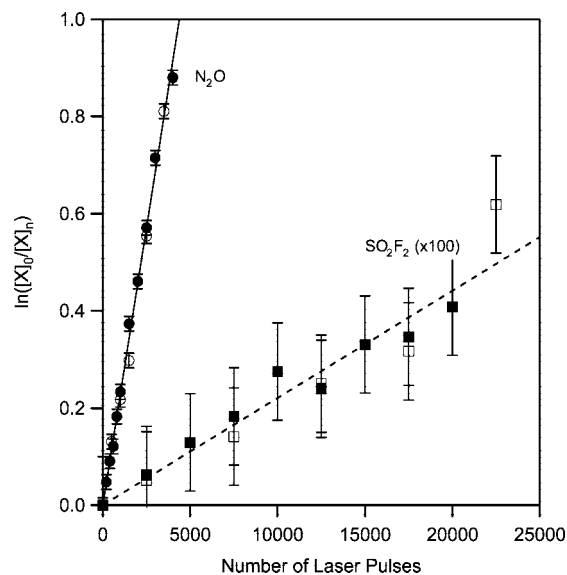
Figure 2. Loss of N_2O (circles) and SO_2F_2 (squares) following pulsed laser photolysis at 193 nm. The SO_2F_2 data has been scaled for clarity (i.e., the number of laser pulses was actually 10 times larger and the ln() values have been multiplied by 10). The losses of N_2O and SO_2F_2 were measured in separate experiments with constant photolysis laser fluence, at 296 K in a N_2 bath gas. The lines are linear least-squares fits to the data, and the ratio of the slopes yield the photolysis quantum yield for SO_2F_2 of 0.02 ± 0.002.

193 nm cross section is a factor of 2 lower. The source for such large discrepancies is at present not known. The spectrum reported in Pradayrol et al. shows diffuse band structure in the wavelength region between 170 and 210 nm. The absorption cross sections in our study were measured at just three discrete wavelengths and are not sufficient to identify any diffuse structure in the SO_2F_2 absorption spectrum. Some of the difference in cross section may, therefore, be due to the differences in the wavelengths used of the cross section measurements.

The quantum yield for the photodissociation of SO_2F_2, Φ, at 193 nm was measured as part of our work. A representative set of quantum yield data, in which the loss of SO_2F_2 following 193 nm pulsed laser photolysis was measured, is shown in Figure 2. Also, included in the figure is a set of laser fluence calibration measurements in which the loss of N_2O, via photodissociation at 193 nm, was measured (see the Experimental Details section). The loss of N_2O scaled linearly with the photolysis laser fluence (varied over the range of 0.8−6.0 mJ cm^{-2} $pulse^{-1}$). The loss of SO_2F_2 was found to be independent of bath gas (N_2, He), the addition of O_2 (10 Torr), and the addition of H_2O (1 Torr). Quantum yield experiments were performed in the two photolysis cells yielded nearly identical results although the total SO_2F_2 loss in the larger volume cell was smaller, a factor of 5, and therefore less accurately measured. The loss of SO_2F_2 per laser pulse was very small due to its small absorption cross section and photolysis quantum yield at 193 nm. These measurements, therefore, required a large number of photolysis laser pulses to produce measurable changes in the SO_2F_2 concentration. No photolysis products were observed via infrared absorption. A linear least-squares analysis of the measured losses of SO_2F_2 and N_2O yielded $\Phi = 0.02 \pm 0.002$, using the 193 nm SO_2F_2 absorption cross section determined in this work, where the uncertainty is the 2σ value from the precision of the fit. The use of the larger 193 nm SO_2F_2 absorption cross section from Pradayrol et al. would yield a SO_2F_2 quantum yield of 0.008.
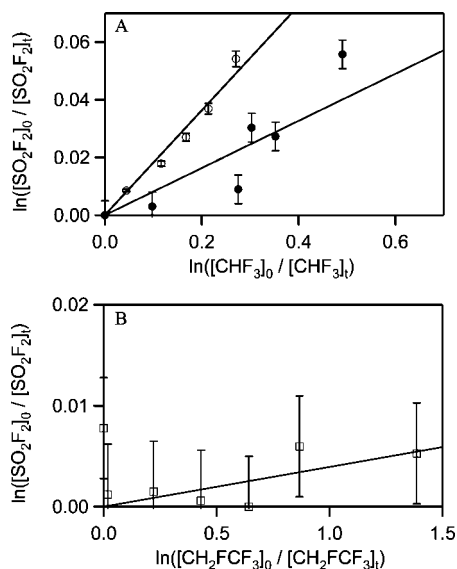
Figure 3. Relative rate data for the OH + $SO_2F_2 \rightarrow$ products, k_1, and Cl + $SO_2F_2 \rightarrow$ products, k_4, reactions with CHF_3 ($k(T) = 6.3 \times 10^{-13}$ exp($-2300/T$) cm^3 molecule^{-1} s^{-1}) and CH_2FCF_3 (HFC-134a); $k(296$ K) = 1.5×10^{-15} cm^3 molecule^{-1} s^{-1}) used for the reference (Ref) compounds, respectively. The k_1 data were measured at 296 (○) and 333 K (●), whereas the k_4 data (□) was obtained at 296 K. The lines are the linear least-squares fits to the data that yield k_1(296 K) = 4.8 $\times 10^{-17}$ cm^3 molecule^{-1} s^{-1}, k_1(333 K) = 5.0 $\times 10^{-17}$ cm^3 molecule^{-1} s^{-1}, and k_4(296 K) = 6.0 $\times 10^{-18}$ cm^3 molecule^{-1} s^{-1}.

OH Rate Coefficient. Representative data from the relative OH rate coefficient measurements for reaction 1, OH + SO_2F_2, are shown in Figure 3. Rate coefficients for reaction 1 were measured at 296 and 333 K using CHF_3 as the reference compound. At both temperatures, the observed loss of SO_2F_2 was small relative to the change in CHF_3 with a 2−6% total change in SO_2F_2 concentration. There was no statistically significant difference in the measured loss of SO_2F_2 observed at the two temperatures. An analysis that included all our measurements (12 experiments at 296 K and 3 experiments at 333 K) yielded k_1(296 K) = (4.9 ± 0.5) $\times 10^{-17}$ cm^3 molecule^{-1} s^{-1} and k_1(333 K) = (5.1 ± 1.2) $\times 10^{-17}$ cm^3 molecule^{-1} s^{-1}. The quoted uncertainties are the 2σ values from the precision of the least-squares analysis.

It is most likely that the small loss of SO_2F_2 observed in our experiments was not in fact due to reaction with OH. First, the possible loss of SO_2F_2 via dark chemistry, including hydrolysis on the walls of the reactor, or loss in the apparatus (circulating pump) was thoroughly checked under all the experimental conditions and found to be negligible, <0.5% SO_2F_2 loss in 3 h. The typical duration of a rate coefficient experiment was ∼30 min. Therefore, the observed loss of SO_2F_2 in our experiment was most likely due to gas-phase chemistry. Second, the negligible temperature dependence observed for the OH + SO_2F_2 rate coefficient is contrary to that expected for a highly endothermic reaction (see the Theoretical Calculations section). Finally, the observed loss of SO_2F_2 may have resulted from the incomplete scavenging of O(^{1}D) radicals by H_2O in the OH radical source chemistry. For the initial concentrations used in our experiments, the ratio [H_2O]/[SO_2F_2] was in the range of 100−200. Under these conditions, a small fraction of the photolytically produced O(^{1}D) would react with SO_2F_2. Dillon et al.[4] reported that reaction 15a has negligible temperature dependence over the range of 225−296 K, consistent with a very efficient gas-phase reaction. There are also several exothermic channels for reaction 15a possible (see the Theoreti-

cal Calculations section). The independence of SO_2F_2 loss observed over the very narrow temperature range used in our experiments is therefore consistent with that expected for reaction 15a. In a separate set of experiments, performed under identical conditions but with no H_2O added, a significant loss of SO_2F_2 (up to 30%) that is due to reaction with O(^{1}D) was observed. This measurement demonstrates our ability to measure SO_2F_2 loss in the apparatus and that the O(^{1}D) reaction leads to loss of SO_2F_2. However, no reaction products were observed from the O(^{1}D) + SO_2F_2 reaction via infrared absorption.

Additionally, the validity of our relative rate approach was confirmed by measuring room temperature rate coefficients for the reaction of OH with CHF_2CF_3 and CHF_3 for which the OH rate coefficients are relatively small but well-established:

$$OH + CHF_2CF_3 \rightarrow products \qquad (19)$$

$$OH + CHF_3 \rightarrow products \qquad (13)$$

The recommended rate coefficients for these reactions are based on relative[8] and absolute[9] rate coefficient measurement techniques and are k_{19}(298 K) = (2.0 ± 0.4) $\times 10^{-15}$ cm^3 molecule^{-1} s^{-1} and k_{13}(298 K) = (2.8 ± 0.6) $\times 10^{-16}$ cm^3 molecule^{-1} s^{-1}.[7] Our measurement results are shown in Figure 4 where CH_2FCF_3 and CHF_2CF_3 were used as reference compounds for the CHF_2CF_3 and CHF_3 reactions, respectively,

$$OH + CH_2FCF_3 \rightarrow products \qquad (20)$$

where k_{20}(298 K) = (4.4 ± 0.1) $\times 10^{-15}$ cm^3 molecule^{-1} s^{-1}.[7] A least-squares analysis yielded k_{19}(296 K) = (2.09 ± 0.20) $\times 10^{-15}$ cm^3 molecule^{-1} s^{-1} and k_{13}(296 K) = (3.46 ± 0.35) $\times 10^{-16}$ cm^3 molecule^{-1} s^{-1}, where the quoted uncertainties are at the 95% level of confidence and include estimated systematic uncertainties (∼9%). Our measured rate coefficients are in agreement, within 5% and 20%, respectively, with the currently recommended values[7] and validate the experimental approach used in this study.

On the basis of our measurements and the possible influence of secondary chemistry leading to the loss of SO_2F_2, we have chosen to report a conservative upper limit for the OH rate coefficient of k_1 < 1 $\times 10^{-16}$ cm^3 molecule^{-1} s^{-1} at 296 and 333 K.

Cl + SO_2F_2 Rate Coefficient. Results from a representative relative rate measurement for reaction 4, Cl + SO_2F_2, are shown in Figure 3. Under all experimental conditions employed in this study, no loss of SO_2F_2 was observed within the precision of the measurements (∼2%). Experiments were performed over a range of initial concentrations, pressure, and photolysis laser fluence as outlined in the Experimental Details section. Experiments were also performed in the absence of the reference compound, CH_2FCF_3, to maximize the possible loss of SO_2F_2. No loss of SO_2F_2 was observed in any experiment. An upper limit for k_4(296 K) of <2.2 $\times 10^{-17}$ cm^3 molecule^{-1} s^{-1} was obtained by taking the 2σ precision of the infrared measurements (2%) as the maximum possible loss of SO_2F_2. After taking into consideration the uncertainty of the reference compound rate coefficient, k_{17}(298 K), we report a conservative upper limit for k_4(296 K) of <5.0 $\times 10^{-17}$ cm^3 molecule^{-1} s^{-1}.

Theoretical Calculations. In order to further evaluate the reactions of OH and Cl with SO_2F_2, reactions 1 and 4, the energetics of a number of possible product channels and the possibility of stable adduct formation were calculated using quantum mechanical molecular methods. Calculations were performed using the Gaussian 98 and Gaussian 03 program suites.[10,11] Standard enthalpies of formation for a number of

TABLE 2: Calculated Enthalpies of Formation, $\Delta_f H°(298.15$ K) (kJ mol^{-1}), for Several Sulfur Species, OH− and Cl−SO$_2$F$_2$ Adducts, and Species Used in Benchmark Calculations

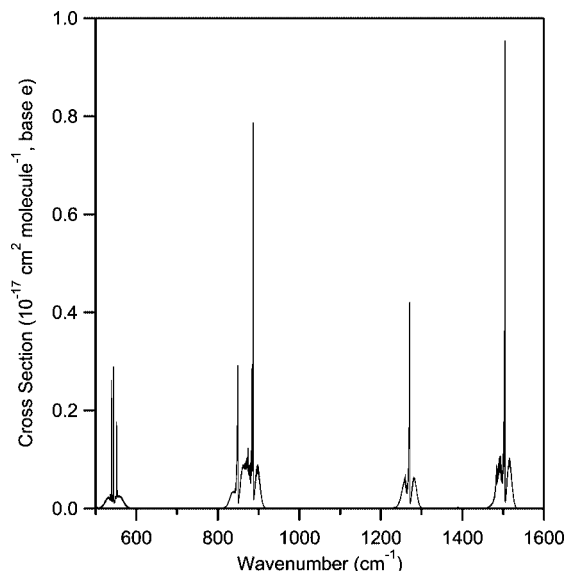| molecule	B3PW91/ aug-cc-pV(T+d)Z	CCSD(T) IB+dDT	CCSD(T) IBa+dDT	CCSD(T) CBSDTQ[a]	literature values[b]
SO$_2$F$_2$	−712.1	−715.9	−727.5	−758.5	−758.6
SOF$_2$	−560.0	−547.1	−560.4	−588.6	−543.9
SO$_3$	−357.2	−351.3	−360.5		−395.8
SO$_2$	−259.9	−257.9	−269.0		−296.8
SO	3.5	24.5	17.3	6.7	5.0
SF$_2$	−277.7	−267.1	−278.4	−293.9	−296.6
F$_2$OSO−HO	−667.7	−682.0			
F$_2$SO−HO	−520.9	−516.0			
HO−SO$_2$F$_2$	−584.8				
HO−SOF$_2$	−550.3	−530.1			
O$_2$FSF−HO	−663.7	−802.1			
OFSF−HO	−512.3	−507.6			
Cl−SO$_2$F$_2$	−586.4				
Cl−SOF$_2$	−426.5				
SO$_3$F	−454.7	−431.0	−443.1		
SO$_2$F	−373.1	−347.4	−358.9	−385.5	
SO$_2$FOH	−692.8	−706.1	−717.5		
SOF	−266.4	−240.2	−251.0	−271.7	
SF	5.8	19.8	12.9	4.2	13.0
F$_2$	13.1	5.2	−0.2	−0.2	0.0
HF	−259.4	−270.8	−273.8	−273.8	−272.5
HO$_2$	5.2	22.6	15.9	15.9	2.1
HOF	−76.6	−83.4	−88.7	−88.7	−98.3
OH	39.6	39.6	36.9	36.9	39.0
ClF	−47.4	−42.4	−49.1	−49.1	−50.3
ClO	93.8	115.6	109.7	109.7	101.2

[a] Calculated values using CCSD(T)/CBSDTQ energies corrected for core−valence effects and scalar-relativistic effects (MVD approach) taken from Grant et al. (ref 17). [b] Values taken from Chase (ref 28) and the NIST Chemistry Webbook (ref 29).
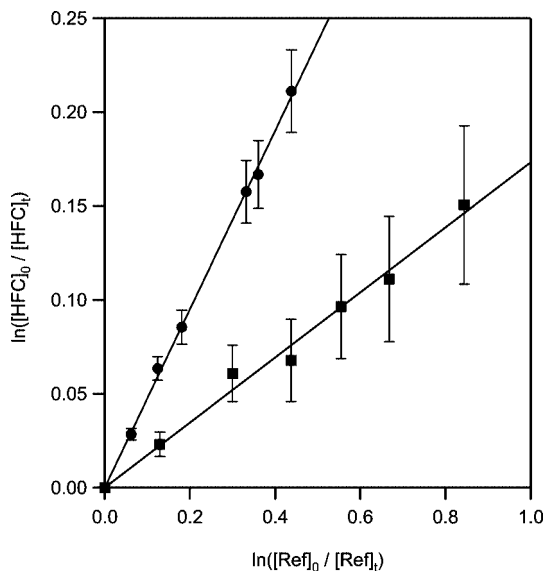
Figure 4. Relative rate data for the OH + CHF$_2$CF$_3$ → products, k_{19}, and OH + CHF$_3$ → products, k_{13}, reactions with CH$_2$FCF$_3$ (k_{20}(298 K) = 4.4 × 10^{-15} cm^3 molecule^{-1} s^{-1}) and CHF$_2$CF$_3$ (k_{19}(298 K) = 2.0 × 10^{-15} cm^3 molecule^{-1} s^{-1}) used as reference compounds, respectively. Both k_{19} (●) and k_{13} (■) data were measured at 296 K. The lines are the linear least-squares fits to the data and yield k_{19}(298 K) = (2.09 ± 0.07) × 10^{-15} cm^3 molecule^{-1} s^{-1} and k_{13}(298 K) = (3.46 ± 0.17) × 10^{-16} cm^3 molecule^{-1} s^{-1} where the uncertainties are the 2σ precision of the fit.

Figure 5. Infrared absorption spectrum of SO$_2$F$_2$, 296 K, measured at 0.125 cm^{-1} resolution in 100 Torr N$_2$ bath gas (available in the Supporting Information).

stable and radical species were calculated. Benchmark calculations for several key small sulfur species were also carried out.

Geometry optimization and vibrational frequency calculations were performed using second-order Møller−Plesset perturbation theory in conjunction with the 6-31G++(d′,p′) basis set. Vibrational frequencies were scaled down by 0.9661. The

optimized molecular structure parameters and vibrational frequencies used in the higher level of theory single-point energy calculations are provided as Supporting Information, Tables S1 and S2.

Absolute electronic energies were calculated employing coupled-cluster theory including single and double excitations, as well as triple excitations in a perturbative manner, CCSD(T). Correlation-consistent basis sets, augmented with a set of tight d-functions for the second-row elements of double- and triple-ζ quality were used in the calculations. In particular, the basis sets used in this work were cc-pV(D+d)Z and cc-pV(T+d)Z,

TABLE 3: Calculated $\Delta_f H$(298.15 K) (kJ mol^{-1}) Values for Possible Product Channels in the Reactions of OH and Cl with SO$_2$F$_2^a$

reaction	B3P86 aug-cc-pV(T+d)Z	CCSD(T) IB+dDT	CCSD(T) IBa+dDT	CCSD(T)CBSDTQ^b	literature value^c
		Bimolecular Channels			
SO$_2$F$_2$ + OH → SO$_2$F + HOF	222.89	245.47	243.03		
SO$_2$F$_2$ + OH → SOF$_2$ + HO$_2$	118.00	151.72	146.21		177.7
SO$_2$F$_2$ + OH → SO$_3$F + HF	−44.14	−25.63	−26.23		
SO$_2$F$_2$ + OH → SO$_2$FOH + F	59.88	49.53	52.58		
SO$_2$F$_2$ + Cl → SO$_2$F + ClF	171.78	204.75	198.18		
SO$_2$F$_2$ + Cl → SOF$_2$ + ClO	126.52	163.05	155.53		194.6
		Adducts			
SO$_2$F$_2$ + OH → HOSO$_2$F$_2$	76.73				
SO$_2$F$_2$ + OH → F$_2$OSOHO	3.13				
SO$_2$F$_2$ + OH → O$_2$FSFHO	7.91				
SO$_2$F$_2$ + Cl → ClSO$_2$F$_2$	2.67				
		Bond Dissociations Energies (Benchmarks)			
SO$_2$F$_2$ → SO$_2$ + F$_2$	476.70	463.16	458.35		461.7
SO$_2$F$_2$ → SO$_2$F + F	433.58	447.86	448.01	452.18	
SO$_2$F$_2$ → SOF$_2$ + O	419.58	417.95	416.33	419.04	463.8
SOF$_2$ → SOF + F	387.57	386.28	388.72	396.12	
SOF$_2$ → SF$_2$ + O	549.98	529.20	531.17	543.72	496.4
SOF$_2$ → SO + F$_2$	590.88	576.72	577.45	581.58	548.9
SO$_3$F → SO$_3$ + F	189.25	159.12	162.01		
SO$_2$F → SO$_2$ + F	204.07	168.95	169.31		
SO$_3$ → SO$_2$ + O	363.71	342.61	340.64		348.1
SO$_2$ → SO + O	533.76	531.51	535.43		551.0
SO → S + O	541.64	501.69	508.90	519.46	521.1
SF$_2$ → SF + F	377.47	366.21	370.69	377.29	363.1
SF → S + F	366.00	336.62	343.46	352.19	369.3

^{a} Geometry optimizations and vibrational frequency calculations were performed at MP2/6-31++G(d′,p′) level of theory and are given in the Supporting Information, whereas density functional (B3P86) an coupled-cluster (CCSD(T)) theories were used for the absolute energy calculations. ^{b} Calculated values using CCSD(T)/CBSDTQ energies corrected for core−valence effects and scalar-relativistic effects (MVD approach) taken from Grant et al. (ref 17). ^{c} Values taken from Chase (ref 28) and the NIST Chemistry Webbook (ref 29).

as well as their diffuse functions augmented variants, aug-cc-pV(D+d)Z and aug-cc-pV(T+d)Z. The zero-point and thermal energies (298.15 K) were derived using harmonic oscillator and the rigid-rotor approximations. Finally, infinite basis (IB) extrapolation was employed.[12−15] The IB method allows the extrapolation of electronic energies to a complete basis set (CBS) limit by using only double- and triple-ζ correlation-consistent basis sets[16] and are denoted as IB+dDT and IBa+dDT, where "a" and "+d" stand for the presence of diffuse functions and extra tight d-functions, respectively, in the basis sets employed. Density functional theory, B3PW91 and B3P86 with the aug-cc-pV(T+d)Z basis set, was used for comparison purposes.

Enthalpies of formation, $\Delta_f H°$(298.15 K) were calculated at the CCSD(T)/IB+dDT, CCSD(T)/IBa+dDT, and B3PW91/aug-cc-pV(T+d)Z levels of theory, and a list of the species included in our calculations and their $\Delta_f H°$(298.15 K) values is given in Table 2. There are limited $\Delta_f H$(298.15 K) experimental values available for many of the species involved in these reactions. In general, the agreement between the calculated and literature values where available are within 15 kJ mol^{-1}. However, the calculated enthalpies for reactions that involve SO$_2$F$_2$ and SOF$_2$, show systematically larger deviations, ∼30 kJ mol^{-1}. This is consistent with the deviations with the literature values for the heats of formation for these species. These differences make little difference in the calculated reaction enthalpy trends mapped out in this work since they are small compared to calculated exothermicities. The reaction channels considered in this work and the $\Delta_r H$(298.15 K) values calculated using CCSD(T)/IB+dDT, CCSD(T)/IBa+dDT and B3PW91/aug-cc-pV(T+d)Z levels of theory are given in Table 3. There is reasonably good

agreement, ±18 kJ mol^{-1}, among the $\Delta_f H$(298.15 K) values obtained using the DFT and coupled-clusters methods.

During the course of our work, Grant et al.[17] reported heats of formation for a series of sulfur containing compounds including SF$_2$, SF$_4$, SF$_6$, SF$_2$O, SF$_2$O$_2$, and SF$_4$O calculated using coupled-cluster theory [CCSD(T)] extrapolated to the CBS limit. The calculated values included corrections for core−valence, scalar-relativistic, and first-order atomic spin−orbit effects and lead to a very accurate set of values. The results reported by Grant et al. overlap to some extent with our study, in particular, with regards to our benchmarking calculations. The results from the Grant et al. study are more accurate than those obtained in our calculations, mainly due to the corrections for core−valence and scalar-relativistic effects. However, the errors in our calculations cancel out, for the most part, when calculating enthalpies of reaction. The results from the Grant et al. study are included in Tables 2 and 3 for comparison with the present results.

The results from our calculations, Table 3, show that product channels involving direct abstraction by OH and Cl from SO$_2$F$_2$ are highly endothermic, $\Delta_r H°_{298.15}$ > 145 kJ mol^{-1}. The exchange reaction, OH + SO$_2$F$_2$ → F + HOSO$_2$F, which is expected to have a very high reaction barrier in the gas phase, is also endothermic. For the OH reaction, the only exothermic product channel was the formation of hydrogen fluoride (HF), OH + SO$_2$F$_2$ → HF + SO$_3$F.

Reactions 1 and 4 are not likely to proceed through adduct formation channels in the gas phase, since no stable intermediate complexes (including hydrogen-bonded and sulfuryl adducts) were found. In other words, the reaction enthalpies calculated
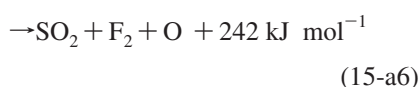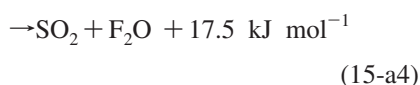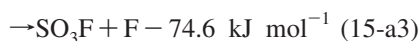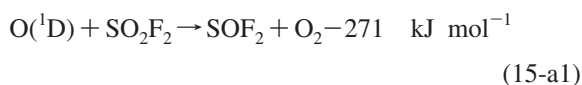
TABLE 4: Summary of SO$_2$F$_2$ Atmospheric Loss Processes and Calculated Atmospheric Lifetimes

SO$_2$F$_2$ losses process	input		lifetime (years)
	value	ref	
ocean uptake		Mühle et al. (ref 1)	40 ± 13
aerosol uptake		Dillon et al. (ref 4)	>100[a]
OH + SO$_2$F$_2$	<1 × 10^{-16b}	this work	>320[c]
Cl + SO$_2$F$_2$	<5 × 10^{-17}	this work	>10 000[d]
O$_3$ + SO$_2$F$_2$	1 × 10^{-23}	Dillon et al. (ref 4)	>24 000[e]
O(^{1}D) + SO$_2$F$_2$	5.8 × 10^{-11}	Dillon et al. (ref 4)	700[f]
UV photolysis alone	$\sigma(\lambda)$ and QY = 1	Pradayrol et al. (ref 5)	225[f]
	$\sigma(\lambda > 190$ nm) and QY	this work	>4700[f g]
	$\sigma(\lambda < 190$ nm) and QY = 1	Pradayrol et al. (ref 5)	
O(^{1}D) + UV photolysis	$k_{15} = 5.8 \times 10^{-11}$	Dillon et al. (ref 4)	630[f]
	$\sigma(\lambda > 190$ nm) and QY	this work	
	$\sigma(\lambda < 190$ nm) and QY = 1	Pradayrol et al. (ref 5)	

[a] Calculated assuming typical marine boundary layer aerosol loading conditions. [b] Rate coefficients are in units of cm^3 molecule^{-1} s^{-1}. [c] [OH] = 1 × 10^6 molecule cm^{-3}. [d] [Cl] = 1 × 10^4 atom cm^{-3}. [e] [O$_3$] = 1 × 10^{12} molecule cm^{-3}. [f] Lifetime calculated in this work using a two-dimensional atmospheric model. [g] The calculated photolysis occurs primarily, >95%, from Lyman-α (121.5 nm) radiation.

for the adduct formation pathways were all endothermic. This implies the absence of any product formation that would proceed through the formation of an adduct. The lack of even weakly bound adduct formation can possibly be explained by the high electrophilicity of sulfur, +6 oxidation state in SO$_2$F$_2$. OH, Cl, and S are all highly electrophilic species, and thus, the lack of a center with high electron density limits the formation of adducts containing even weak S···O—H or S···Cl bonds. Hydrogen-bonded adducts were also found to be unstable as the high requirements of sulfur for electron density inhibits OH from approaching the fluorine or oxygen atoms in SO$_2$F$_2$.

The thermochemical parameters obtained in this work, Table 2, can also be used to evaluate possible reactive channels in reaction 15a

$$O(^1D) + SO_2F_2 \rightarrow SOF_2 + O_2 - 271 \quad kJ \ mol^{-1}$$

$$(15\text{-}a1)$$

$$\rightarrow SO_3 + F_2 - 106 \ kJ \ mol^{-1} \quad (15\text{-}a2)$$

$$\rightarrow SO_3F + F - 74.6 \ kJ \ mol^{-1} \quad (15\text{-}a3)$$

$$\rightarrow SO_2 + F_2O + 17.5 \ kJ \ mol^{-1}$$

$$(15\text{-}a4)$$

$$\rightarrow SO_2F + FO + 40 \ kJ \ mol^{-1} \quad (15\text{-}a5)$$

$$\rightarrow SO_2 + F_2 + O + 242 \ kJ \ mol^{-1}$$

$$(15\text{-}a6)$$

where the heats of reaction, $\Delta_r H(296$ K), given are calculated using data from Table 2, and heats of formation are from Sander et al.[7] Dillon et al.[4] reported that ~45% of O(^{1}D) loss in the interaction with SO$_2$F$_2$ leads to chemical reaction, i.e., loss of SO$_2$F$_2$. There are several exothermic channels available in reaction 15a including O-atom abstraction, 15-a1, the formation of stable molecular products, 15-a2, and atom exchange, 15-a3. In the experiments performed in the present study, infrared absorption of reaction mixtures, we were not able to identify the products in reaction 15a.

In summary, our theoretical calculations clearly show that all possible direct abstraction channels in the reactions of Cl and OH with SO$_2$F$_2$ are highly endothermic and, therefore, unlikely to occur with significant rate coefficients under atmospheric conditions. In addition, the exchange of OH with an F atom in SO$_2$F$_2$ was calculated to be ~58 kJ mol^{-1}

endothermic. Our calculations also investigated the possibility of Cl and OH + SO$_2$F$_2$ adduct formation. However, no stable intermediate complexes (adducts) were found. This result implies that adduct formation is not an efficient processes for the removal of SO$_2$F$_2$ from the atmosphere. The only exothermic channel found was for the OH + SO$_2$F$_2$ → HF + SO$_3$F reaction, $\Delta_r H(298.15$ K) ≈ −26 kJ mol^{-1}. This reaction, however, would most likely need to proceed through the formation of an unstable (HO···SO$_2$F$_2$) adduct and therefore be highly unlikely. In addition, there was no evidence for the formation of HF in our laboratory experiments. The theoretical calculations support our experimental observations and the reported upper limits for k_1 (<10^{-16} cm^3 molecule^{-1} s^{-1}) and k_4 (<5 × 10^{-17} cm^3 molecule^{-1} s^{-1}).

Atmospheric Implications

Atmospheric Lifetime. On the basis of our laboratory studies and the analysis of SO$_2$F$_2$ field observations,[1] it is clear that SO$_2$F$_2$ is a long-lived atmospheric trace species. A summary of the SO$_2$F$_2$ loss processes and associated atmospheric lifetimes is given in Table 4.

In this work, we determined an upper limit for the rate coefficient for reaction 1, $k_1(298$ K) < 1 × 10^{-16} cm^3 molecule^{-1} s^{-1}. This value is in agreement with the upper limit of 1 × 10^{-15} cm^3 molecule^{-1} s^{-1} recently reported by Dillon et al.,[4] but the uncertainties in this parameter have been considerably reduced by the results presented in this work. The tropospheric lifetime of SO$_2$F$_2$, with respect to its reaction with OH, τ_{OH}, is >300 years for an OH radical concentration of 10^6 molecule cm^{-3}, which is a representative average tropospheric concentration.[18] For the reaction of SO$_2$F$_2$ with Cl atoms, we determined an upper limit for the rate coefficient, $k_4(298$ K) < 5 × 10^{-17} cm^3 molecule^{-1} s^{-1}. The atmospheric lifetime of SO$_2$F$_2$ with respect to loss by Cl atom reaction, τ_{Cl}, is >10 000 years for an tropospheric Cl atom concentration of 10^4 cm^{-3}, which is currently thought to be representative of the Cl atom concentration in the free troposphere.[19] We should note that the tropospheric Cl atom concentration is poorly known at present and is likely dependent on time and location. Therefore, the τ_{Cl} value given here should be considered as only an approximation. In any case, however, the gas-phase Cl atom reaction likely represents a negligible atmospheric loss process for SO$_2$F$_2$.

Atmospheric loss via reaction with O(^{1}D) and by UV photolysis are primarily stratospheric loss processes for SO$_2$F$_2$. Stratospheric loss processes alone lead to long atmospheric

Atmospheric Chemistry and GWP of SO$_2$F$_2$

J. Phys. Chem. A, Vol. xxx, No. xx, XXXX **I**

TABLE 5: Infrared Absorption Band Strengths for SO$_2$F$_2$ at 296 K

integration range (cm^{-1})	band strength (10^{-17} cm^2 molecule^{-1} cm^{-1})	
	Dillon et al. (ref 4)[a]	this work[b]
500.9−592.5	1.4	1.34 ± 0.05
800.8−927.6	5.7	5.84 ± 0.02
1211.1−1321.5	2.5	2.61 ± 0.01
1448.8−1542.3	4.0	4.17 ± 0.01

[a] The 2σ uncertainties are reported to be <10%. [b] The quoted uncertainties are obtained from the 2σ precision of the slope of the linear least-squares analysis of the measured integrated absorption versus SO$_2$F$_2$ concentration.

lifetimes, at least decades, due to the slow turnover rate of the atmosphere through the stratosphere. The NOCAR two-dimensional model[20] was used to compute the stratospheric lifetime of SO$_2$F$_2$, which is estimated to be 630 years. This loss is dominated by reaction with O(^{1}D). Therefore, reaction with O(^{1}D) and UV photolysis are minor atmospheric loss processes for SO$_2$F$_2$.

In conclusion, all gas-phase loss processes for SO$_2$F$_2$ studied to date are slow and lead to long atmospheric lifetimes for SO$_2$F$_2$. The most likely SO$_2$F$_2$ removal process is via ocean uptake as recently pointed out by Mühle et al.[1] Mühle et al. reported a SO$_2$F$_2$ globally averaged lifetime of 36 ± 11 years and a lifetime with respect to uptake by the ocean of 40 ± 13 years. Mühle et al. obtained these lifetimes using an inversion model that included air−sea exchange with the oceanic mixed layer combined with hydrolysis rates calculated using the parameters given by Cady and Misra.[21] Note that an ocean uptake lifetime of 40 years is significantly shorter than the value recently reported by Dillon et al.[4] Dillon et al. did not account for air−sea exchange in their simple uptake calculation, and this primarily accounts for the discrepancies in the reported ocean uptake lifetimes; see Mühle et al.[1] for a detailed discussion. Gas-phase removal processes for SO$_2$F$_2$ would therefore not exceed 10% of the loss due to ocean uptake and may be much smaller.

Global Warming Potential. The infrared absorption spectrum of SO$_2$F$_2$, Figure 5, was measured as part of this work. The peak cross sections of the Q-branches were found to be dependent on the resolution of the measurement with an increase in peak cross section observed at higher resolution. The SO$_2$F$_2$ band strengths are given in Table 5 and were found to be independent of the resolution and total pressure of the measurement. The SO$_2$F$_2$ infrared spectrum has several strong vibrational bands that fall within the atmospheric window and make SO$_2$F$_2$ an efficient atmospheric greenhouse gas. The present results are in good agreement with those from previous studies and are appropriate for atmospheric model calculations.[4,22,23]

The GWP of a gas is a measure of the time-integrated radiative forcing to the climate system of a pulse of the gas relative to a baseline (usually taken to be CO$_2$). This allows the climatic impact of the emission of one gas relative to another to be quantified.[24] We computed the radiative efficiency of SO$_2$F$_2$ using an accurate line-by-line (LBL) radiative transfer code.[25] For a comparison study of this radiative transfer code versus others see Forster et al.[26] The LBL code uses the absorption spectra of SO$_2$F$_2$ measured in this work, along with the line parameters for the other gases taken from the HITRAN-2000 database. A constant profile (both vertically and meridionally) of SO$_2$F$_2$ is assumed in the calculation as is commonly done for GWP calculations. For gases reasonably well mixed

in the troposphere this usually amounts to not more than a 10% error in the radiative forcing.[27] The radiative efficiency for SO$_2$F$_2$ calculated using the spectra shown in Figure 2 is 0.222 W m^{-2} ppb^{-1}. The GWP for SO$_2$F$_2$ is 7642, 4780, and 1540 for the 20, 100, and 500 year time horizons, for an SO$_2$F$_2$ atmospheric lifetime of 36 years. This GWP calculation uses the same integrated radiative forcing of CO$_2$ used in WMO 2007 and therefore can be compared with the GWPs reported there. SO$_2$F$_2$ is an efficient greenhouse gas, its GWP is similar to those of chlorofluorocarbons (CFCs),[24] and it could have a significant climatic impact if present in the atmosphere in sufficient abundance.

Conclusions

SO$_2$F$_2$ is a long-lived trace species that is currently present in the atmosphere at levels of ~1.5 ppt. The impact of SO$_2$F$_2$ on the environment and climate is dependent on its atmospheric lifetime. In this study, we have established upper limits for the gas-phase reaction of SO$_2$F$_2$ with OH radicals and Cl atoms. UV absorption cross section and photodissociation quantum yield measurements also established that UV photolysis is a negligible atmospheric loss process for SO$_2$F$_2$. The stratospheric lifetime of SO$_2$F$_2$ was calculated to be 630 years using literature values for the O(^{1}D) + SO$_2$F$_2$ rate coefficient[4] and SO$_2$F$_2$ UV absorption cross sections[5] combined with the UV cross section data and quantum yields measured in this work.

Theoretical quantum calculations were used to evaluate the thermochemistry and possible reaction channels for the OH and Cl atom reactions with SO$_2$F$_2$. The calculated thermochemistry for the OH and Cl reactions with SO$_2$F$_2$ establishes that the most likely bimolecular reaction channels are highly endothermic. In addition, the formation of stable OH or Cl adducts with SO$_2$F$_2$ were also found to be unlikely. The results from our theoretical calculations are consistent with the experimental evidence for the low chemical reactivity of SO$_2$F$_2$.

The atmospheric lifetime of SO$_2$F$_2$ is at present relatively uncertain with the best available estimate being 36 ± 11 years based on a model calculation that includes results from the present study and finds ocean uptake to be the primary atmospheric loss process.[1] On the basis of this globally averaged SO$_2$F$_2$ atmospheric lifetime and the infrared cross sections measured in this work, the GWP of SO$_2$F$_2$, on a 100 year time horizon, was calculated to be 4780. Further atmospheric monitoring of this recently discovered trace gas and its global distribution would most likely enable improved estimates of the lifetime to be made in the future. However, it is clear from the information currently available that the GWP for SO$_2$F$_2$ is significant although the uncertainty, ±30%, is large. A shorter (longer) SO$_2$F$_2$ lifetime than used in our present calculation will result in a smaller (larger) GWP for SO$_2$F$_2$. The radiative forcing of SO$_2$F$_2$ is currently small, 3.3 × 10^{-4} mW m^{-2}, but requires consideration in the future use of SO$_2$F$_2$.

Supporting Information Available: Infrared absorption cross section data of SO$_2$F$_2$ and optimized calculated geometry and vibrational frequencies, performed at the MP2/6-31++G(d′,p′) level of theory, for the species in Table 3. This material is available free of charge via the Internet at http://pubs.acs.org.

References and Notes

(1) Mühle, J.; Huang, J.; Weiss, R. F.; Prinn, R. G.; Miller, B. R.; Salameh, P. K.; Harth, C. M.; Fraser, P. J.; Porter, L. W.; Greally, B. R.; O'Doherty, S.; Simonds, P. G. *J. Geophys. Res.*, submitted for publication, **2008**.

(2) Sulfuryl fluoride (Vikane) risk characterization document, environmental fate; California Environmental Protection Agency, 2006. http://www.cdpr.ca.gov.

(3) Assesment report: Sulfuryl fluoride, toxicology and chemical substances; European Chemicals Bureau, 2006. http://ecb.jrc.it.

(4) Dillon, T. J.; Horowitz, A.; Crowley, J. N. *Atmos. Chem. Phys.* **2008**, *8*, 1547.

(5) Pradayrol, C.; Casanovas, A. M.; Deharo, I.; Geuelfucci, J. P.; Casanovas, J. *J. Phys. III* **1996**, *6*, 603.

(6) Gierczak, T.; Burkholder, J. B.; Bauerle, S.; Ravishankara, A. R. *Chem. Phys.* **1998**, *231*, 229.

(7) Sander, S. P.; Friedl, R. R.; Golden, D. M.; Kurylo, M. J.; Moortgat, G. K.; Keller-Rudek, H.; Wine, P. H.; Ravishankara, A. R.; Kolb, C. E.; Molina, M. J.; Finlayson-Pitts, B. J.; Huie, R. E.; Orkin, V. L. Chemical kinetics and photochemical data for use in atmospheric studies; JPL Publication 06-2; Jet Propulsion Laboratory: Pasadena, CA, 2006; Vol. Evaluation Number 15.

(8) Hsu, K.-J.; DeMore, W. B. *J. Phys. Chem.* **1995**, *99*, 1235.

(9) Talukdar, R.; Mellouki, A.; Gierczak, T.; Burkholder, J. B.; McKeen, S. A.; Ravishankara, A. R. *J. Phys. Chem.* **1991**, *95*, 5815.

(10) Frisch, M. J.; Trucks, G. W.; Schlegel, H. B.; Scuseria, G. E.; Robb, M. A.; Cheeseman, J. R.; Montgomery, J. A., Jr.; Vreven, T.; Kudin, K. N.; Burant, J. C.; Millam, J. M.; Iyengar, S. S.; Tomasi, J. J.; Barone, V.; Mennucci, B.; Cossi, M.; Scalmani, G.; Rega, N.; Petersson, G. A.; Nakatsuji, H.; Hada, M.; Ehara, M.; Toyota, K.; Fukuda, R.; Hasegawa, J.; Ishida, M.; Nakajima, T.; Honda, Y.; Kitao, O.; Nakai, H.; Klene, M.; Li, X.; Knox, J. E.; Hratchian, H. P.; Cross, J. B.; Adamo, C.; Jaramillo, J.; Gomperts, R.; Stratmann, R. E.; Yazyev, O.; Austin, A. J.; Cammi, R.; Pomelli, C.; Ochterski, J. W.; Ayala, P. Y.; Morokuma, K.; Voth, A.; Salvador, P.; Dannenberg, J. J.; Zakrzewski, V. G.; Dapprich, S.; Daniels, A. D.; Strain, M. C.; Farkas, O.; Malick, D. K.; Rabuck, A. D.; Raghavachari, K.; Foresman, J. B.; Ortiz, J. V.; Cui, Q.; Baboul, A. G.; Clifford, S.; Cioslowski, J.; Stefanov, B. B.; Liu, G.; Liashenko, A.; Piskorz, P.; Komaromi, I.; Martin, R. L.; Fox, D. J.; Keith, T.; Al-Laham, M. A.; Peng, C. Y.; Nanayakkara, A.; Challacombe, M.; Gill, P. M. W.; Johnson, B.; Chen, W.; Wong, M. W.; Gonzalez, C.; Pople, J. A. Gaussian 03, revision B.02; Gaussian Inc.: Pittsburgh, PA, 2003.

(11) Frisch, M. J.; Trucks, G. W.; Schlegel, H. B.; Scuseria, G. E.; Robb, M. A.; Cheeseman, J. R.; Zakrzewski, V. G.; Petersson, G. A.; Montgomery, J. A., Jr.; Stratmann, R. E.; Burant, J. C.; Dapprich, S.; Millam, J. M.; Daniels, A. D.; Kudin, K. N.; Strain, M. C.; Farkas, O.; Tomasi, J.; Barone, V.; Cossi, M.; Cammi, R.; Mennucci, B.; Pomelli, C.; Adamo, C.; Clifford, S.; Ochterski, J.; Petersson, G. A.; Ayala, P. Y.; Cui, Q.; Morokuma, K.; Malick, D. K.; Rabuck, A. D.; Raghavachari, K.; Foresman, J. B.; Cioslowski, J.; Ortiz, J. V.; Stefanov, B. B.; Liu, G.; Liashenko, A.; Piskorz, P.; Komaroni, I.; Gomperts, R.; Martin, R. L.; Fox, D. J.; Keith, T. A.; Al-Laham, M. A.; Peng, C. Y.; Nanayakkara, A.; Gonzalez, C.; Challacombe, M.; Gill, P. M. W.; Johnson, B. G.; Chen, W.; Wong, M. W.; Andreas, J. L.; Head-Gordon, M.; Replogle, E. S.; Pople, J. A. Gaussian 98, revision A9; Gaussian Inc.: Pittsburg, PA, 1998.

(12) Dunning, T. H., Jr.; Peterson, K. A.; Wilson, A. K. *J. Chem. Phys.* **2001**, *114*, 9244.

(13) Fast, P. L.; Sanchez, M. L.; Truhlar, D. G. *J. Chem. Phys.* **1999**, *111*, 2921.

(14) Truhlar, D. G. *Chem. Phys. Lett.* 1998, *294*, 45.

(15) Wilson, A. K.; Dunning, T. H., Jr. *J. Phys. Chem. A* **2004**, *108*, 3129.

(16) Lazarou, Y. G.; Papadimitriou, V. C.; Prosmitis, A. V.; Papagiannakopoulos, P. *J. Phys. Chem. A* **2002**, *106*, 11502.

(17) Grant, D. J.; Matus, M. H.; Switzer, J. R.; Dixon, D. A.; Francisco, J. S.; Christe, K. O. *J. Phys. Chem. A* **2008**, *112*, 3145; doi: 10.1021/jp710373e S1089-5639(71)00373-6.

(18) Prinn, R. G.; Huang, J.; Weiss, R. F.; Cunnold, D. M.; Fraser, P. J.; Simmonds, P. G.; McCulloch, A.; Harth, C.; Salameh, P.; O'Doherty, S.; Wang, R. H. J.; Porter, L.; Miller, B. R. *Science* **2001**, *292*, 1882.

(19) Platt, U.; Allen, W.; Lowe, D. *Atmos. Chem. Phys.* **2004**, *4*, 2283.

(20) Portmann, R. W.; Brown, S. S.; Gierczak, T.; Talukdar, R. K.; Burkholder, J. B.; Ravishankara, A. R. *Geophys. Res. Lett.* **1999**, *26*, 2387.

(21) Cady, G. H.; Misra, S. *Inorg. Chem.* **1974**, *13*, 837.

(22) Hunt, G. R.; Wilson, M. K. *Spectrochim. Acta* **1960**, *16*, 570.

(23) Perkins, W. D.; Wilson, M. K. *J. Chem. Phys.* **1952**, *20*, 1791.

(24) Scientific Assessment of Ozone Depletion: 2006, Global Ozone Research and Monitoring Project; WMO (World Meteorological Organization): Geneva, Switzerland, 2007.

(25) Portmann, R. W.; Solomon, S.; Fishman, J.; Olson, J. R.; Kiehl, J. T.; Briegleb, B. *J. Geophys. Res.* **1997**, *102*, 9409.

(26) Forster, P. M. de F.; Burkholder, J. B.; Clerbaux, C.; Coheur, P. F.; Dutta, M.; Gohar, L. K.; Hurley, M. D.; Myhre, G.; Portmann, R. W.; Shine, K. P.; Wallington, T. J.; Wuebbles, D. *J. Quant. Spectrosc. Radiat. Transfer* **2005**, *93*, 447.

(27) Pinnock, S.; Hurley, M. D.; Shine, K. P.; Wallington, T. J.; Smyth, T. J. *J. Geophys. Res.* **1995**, *100*, 23.

(28) Chase, M. W. NIST−JANAF Themochemical Tables, 4th ed. *J. Phys. Chem. Ref. Data, Monogr.* **1998**, *9*, 1.

(29) NIST Chemistry WebBook, NIST Standard Reference Database; Vol. 69. http://webbook.nist.gov/chemistry.